applied sciences

MDPI

Article

Three-Dimensional Structure Reconstruction System of Nasal Cavity Based on a Short-Source Acoustic Tube

Xiaoqin Lian [1,2], Guochun Ma [1,2], Chao Gao [1,2,*], Yuqiao Wang [1,2], Yelan Wu [1,2], Jin Li [1,2], Wenyang Guan [1,2] and Yonggang Gong [1,2]

[1] School of Computer and Artificial Intelligence, Beijing Technology and Business University, Beijing 100048, China; lianxq@th.btbu.edu.cn (X.L.); 2230601019@st.btbu.edu.cn (G.M.); 2130061029@st.btbu.edu.cn (Y.W.); wuyel@th.btbu.edu.cn (Y.W.); jinli@btbu.edu.cn (J.L.); guanwenyang@btbu.edu.cn (W.G.)

[2] Key Laboratory of Industrial Internet and Big Data, China National Light Industry, Beijing Technology and Business University, Beijing 100048, China

* Correspondence: gaochao9158@btbu.edu.cn

Abstract: The nasal cavity three-dimensional structure reconstruction is significant for the diagnosis and treatment of nasal and nasopharynx diseases. Currently, most systems for nasal cavity three-dimensional structure reconstruction are based on a long-source acoustic tube. However, the long-source acoustic tube has the weaknesses of low portability and high cost. To address these issues, a nasal cavity three-dimensional structure reconstruction system based on a short-source acoustic tube was designed in this research. The designed system comprises the lower computer of a nasal acoustic signal acquisition device and the upper computer of nasal acoustic signal analysis software. The lower computer of a nasal acoustic signal acquisition device consists of a signal processing unit, a detection unit, a microcontroller, and a USB communication interface. It is used to collect the original acoustic signal in the nasal cavity. The upper computer of nasal acoustic signal analysis software consists of the nasal cavity acoustic signal preprocessing method and the nasal cavity three-dimensional structure hierarchical reconstruction method. The nasal cavity acoustic signal preprocessing method is used to eliminate the DC offset component and suppress the high-frequency noise. Then, the nasal cavity three-dimensional structure hierarchical reconstruction method is used to establish the relationship between the cross-sectional area of the nasal cavity and the depth of the nasal cavity. In order to verify the effectiveness of the system designed in this research, the straight tube model and the simulated nasal cavity model were selected as test subjects, and the depth–cross-sectional area was selected as the evaluation indicator of the accuracy of the nasal cavity three-dimensional structure reconstruction result. The experimental results show that the root mean squared error and the mean relative error of the depth–cross-sectional area were reduced from 0.6284 cm^2 to 0.0201 cm^2 and 47.6467% to 1.8248%, respectively, under the straight tube model by using the nasal cavity acoustic signal preprocessing method. The root mean squared error and the mean relative error of the depth–cross-sectional area were reduced from 4.7730 cm^2 to 0.1510 cm^2 and 107.8128% to 3.3096%, respectively, under the simulated nasal cavity model. Meanwhile, this system can increase the effective measurement depth of the nasal cavity from 7 cm to 13 cm based on the preprocessing method. The results demonstrated that the designed system can not only reconstruct and visualize a nasal cavity three-dimensional structure with high precision but also generate comprehensive test reports. Therefore, this system can provide a basis for further auxiliary diagnosis of the disease and facilitate doctors in explaining the physiological structure of the nasal cavity to patients.

Keywords: nasal cavity; three-dimensional structure reconstruction; short-source acoustic tube; auxiliary diagnosis

check for updates

Citation: Lian, X.; Ma, G.; Gao, C.; Wang, Y.; Wu, Y.; Li, J.; Guan, W.; Gong, Y. Three-Dimensional Structure Reconstruction System of Nasal Cavity Based on a Short-Source Acoustic Tube. *Appl. Sci.* **2024**, *14*, 369. https://doi.org/10.3390/app14010369

Academic Editor: Mihailo Ristic

Received: 30 November 2023
Revised: 26 December 2023
Accepted: 28 December 2023
Published: 30 December 2023

Copyright: © 2023 by the authors. Licensee MDPI, Basel, Switzerland. This article is an open access article distributed under the terms and conditions of the Creative Commons Attribution (CC BY) license (https://creativecommons.org/licenses/by/4.0/).

1. Introduction

In recent years, nasal obstruction, as a common disease, has seriously affected people's physical health and quality of life. This symptom may be caused by various diseases, including rhinitis, sinusitis, deviation of the nasal septum, nasal polyps, tumors of the nasal cavity and sinuses, etc. The treatment methods for each disease vary greatly. Therefore, it is important to accurately diagnose the cause of nasal obstruction. As obstructive nasal diseases often change the internal structure of the nasal cavity, three-dimensional nasal cavity reconstruction can be used to quickly assist in the diagnosis of obstructive nasal diseases [1–3].

Currently, the detection principles of nasal cavity three-dimensional structure reconstruction are mainly divided into the layered scanning method and the acoustic wave reflection method. The layered scanning method mainly includes a CT scan and an MRI of the nasal cavity [4,5], both of which require a higher examination environment. The advantage of CT is that it has good tissue density resolution, and there is no overlapping of tissues in the scanning image. However, if the lesion is too mild, a CT examination is prone to misdiagnosis or omission. In addition, CT has poor contrast of soft tissues, which may increase the risk of misdiagnosis [6–8]. The advantage of MRI is that it has better resolution of soft tissues, but the imaging result is a cross-section of the nasal cavity in different directions, which lacks a description of the overall structure of the nasal cavity. In summary, the drawbacks of the layered scanning method include its complexity, high cost, and long detection time, limiting its portability.

Based on the acoustic wave reflection method, the nasal cavity three-dimensional structure reconstruction can effectively overcome the drawbacks of the layered scanning method, which is mainly divided into the short-source acoustic tube [9,10] and the long-source acoustic tube [11] according to the length of the acoustic tube. Marshall et al. [12] utilized the long-source acoustic tube for nasal cavity three-dimensional structure reconstruction. By introducing a constraint factor to eliminate the high-frequency noise, the signal-to-noise ratio of the high-frequency part of the input impulse response was improved, significantly enhancing the precision of the nasal cavity three-dimensional structure reconstruction. Aijun Li et al. [13] analyzed the reason for the direct current (DC) offset component in the acoustic reflection method based on a long-source acoustic tube, after introducing the constraint factor. The accuracy of the final nasal cavity three-dimensional reconstruction results was improved by eliminating the DC offset component.

The advantage of the long-source acoustic tube reflection method is that it is convenient to separate the incident and reflected waves, thus improving the accuracy of the nasal cavity three-dimensional reconstruction results, but the long-source acoustic tube is inconvenient to operate and less portable. In contrast, the short-source acoustic tube reflection method uses the short-source acoustic tube, which is convenient to operate and more portable for collecting the data, but the difficulty of separating the incident and reflected waves is increased. Ultimately, the accuracy of the final nasal cavity three-dimensional structure reconstruction results by using the short-source acoustic tube reflection method is lower than that of the long-source acoustic tube reflection method. Marshall [14] addressed the challenge of separating incident and reflected waves in the short-source acoustic tube reflection method by using the acoustic signals collected by the long-source acoustic tube as an auxiliary to separate the incident and reflected waves. This approach effectively resolved the challenge and subsequently enhanced the accuracy of the final nasal cavity three-dimensional structure reconstruction results. However, in this method, the long-source acoustic tube is still needed to assist in separating the incident and reflected waves, and the effects of the DC offset component and the high-frequency noise are not taken into account.

Aiming at overcoming the shortcomings of the current short-source acoustic tube reflection method, this research designed a system for nasal cavity three-dimensional structure reconstruction based on the short-source acoustic tube. The main research contents include the following: (1) A nasal acoustic signal acquisition device was constructed

for acquiring the original nasal acoustic signals. (2) Incident and reflected waves were separated based on the propagation characteristics of the short-source acoustic tube, and acoustic signals were preprocessed, including the elimination of the DC offset component and the introduction of a constraint factor to suppress high-frequency noise. (3) The nasal cavity two-dimensional depth–cross-sectional area curves were generated, and the nasal cavity three-dimensional structure reconstruction model was performed. (4) The software platform of the upper computer was constructed to visualize and analyze the results of the nasal cavity structure reconstruction.

2. Nasal Cavity Three-Dimensional Structure Reconstruction System

In this research, a nasal cavity three-dimensional structure reconstruction system was designed based on the short-source acoustic tube, which is mainly composed of the lower computer of a nasal acoustic signal acquisition device and the upper computer of nasal acoustic signal analysis software. The architecture of the nasal cavity three-dimensional structure reconstruction system is shown in Figure 1.

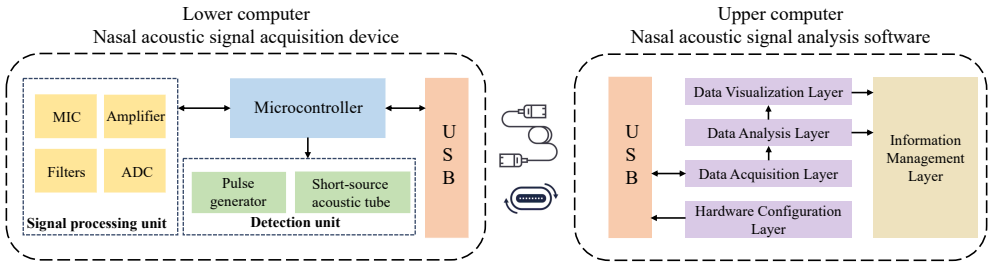


Figure 1. Nasal cavity three-dimensional structure reconstruction system architecture diagram.

The lower computer of the nasal acoustic signal acquisition device consists of a signal processing unit, a detection unit, a microcontroller, and a USB communication interface. It is used to collect the original acoustic signal in the nasal cavity. The upper computer of the nasal acoustic signal analysis software consists of a hardware configuration layer, a data acquisition layer, a data analysis layer, a data visualization layer, and an information management layer. At the same time, the upper computer of the nasal acoustic signal analysis software acts as the initiator of the acquisition commands and the receiver of the acquired data and is used to analyze and visualize the nasal cavity two-dimensional depth–cross-sectional area curves and the nasal cavity three-dimensional structure reconstruction model.

The workflow of the nasal cavity three-dimensional structure reconstruction system is as follows: firstly, the acquisition command is given by the upper computer software. After the command is received by the lower computer, the microcontroller controls the detection unit to emit pulsed acoustic waves. Then, the pulsed acoustic waves are propagated and reflected along the short-source acoustic tube. Subsequently, the reflected waves are received and conditioned by the signal processing unit as the original nasal acoustic signals, processed by the microcontroller, and then sent to the upper computer for further processing via the USB communication interface. After receiving the original nasal acoustic signals, the upper computer software analyzes the signals using the data analysis layer and calculates the cross-sectional area values corresponding to the different depths of the nasal cavity. Then, the depth–cross-sectional area values are displayed using a variety of visualization methods in the data visualization layer. Finally, the depth–cross-sectional area values are stored uniformly in the information management layer based on personal information such as the tester's name and test time.

2.1. The Lower Computer of Nasal Acoustic Signal Acquisition Device

The structure of the lower computer nasal acoustic signal acquisition device is shown in Figure 2. Its basic structure includes a detection unit composed of a pulse generator and a short-source acoustic tube; a signal processing unit composed of an MIC, an amplifier,

a 10 KHz low-pass filter, and an A/D analog-to-digital converter; a microcontroller; a USB communication interface [15]. These four components, respectively, implement the functions of pulsed acoustic wave generation and reflection, original nasal acoustic signal acquisition and quantification, control of the acquisition device, and data transmission. The short-source acoustic tube consists of a hollow glass tube with an embedded microphone; the glass tube is 40 cm long, and the microphone is embedded in the side of the glass tube.

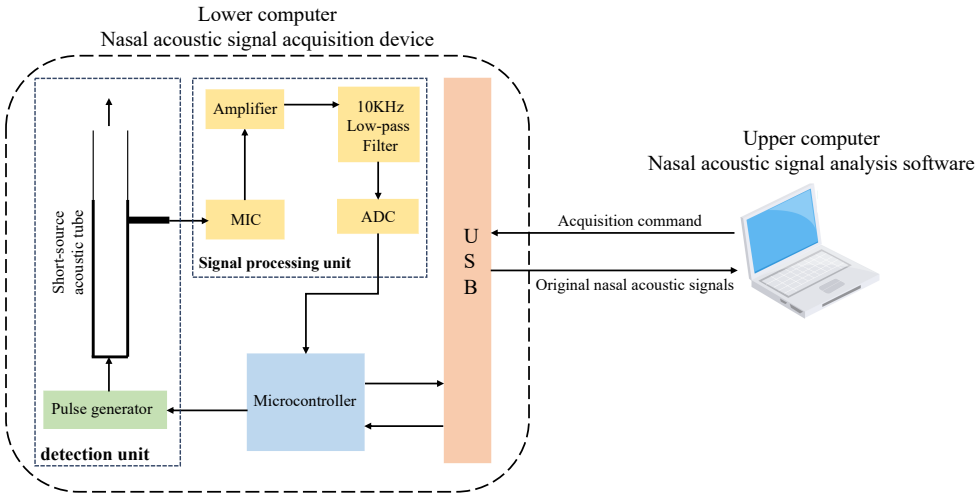


Figure 2. Lower computer hardware architecture diagram.

The workflow of the lower computer nasal acoustic signal acquisition device is as follows: the upper computer software sends acquisition commands to the lower computer through the USB communication interface. Upon receiving the command, the microcontroller in the lower computer sends an enable signal to the pulse generator, causing it to generate pulsed acoustic waves. The pulsed acoustic waves propagate and reflect along the short-source acoustic tube and are finally received by the microphone. After being conditioned through the circuit, the original nasal acoustic signal is obtained. The signal is then quantized by the A/D converter and relayed to the upper computer software via the USB communication interface for further processing.

2.2. The Upper Computer of Nasal Acoustic Signal Analysis Software

The upper computer software architecture is shown in Figure 3. The software consists of five main parts, from bottom to top: the hardware configuration layer, the data acquisition layer, the data analysis layer, the data visualization layer, and the information management layer.

- In the hardware configuration layer, the ID of the acquisition card can be bound to the lower computer. The sampling rate and sampling time of the acquisition card can be configured through parameter configuration. At the same time, different starting cross-sectional areas and constraint factors can be configured according to the acoustic tubes used, providing robust support for the data acquisition layer even when changing the physical size of the tube.
- The data acquisition layer primarily controls the data acquisition process. It supports the single acquisition mode and the automatic multiple acquisitions mode. Each mode can utilize the self-check function, which includes assessing the intensity of the original nasal acoustic signal to avoid using a damaged short-source acoustic tube, which might lead to unusable detection results. This function ensures data reliability and provides a high-quality original nasal acoustic signal for the data analysis layer.
- The data analysis layer is the core of the software. The nasal cavity depth–cross-sectional area values can be calculated accurately by applying the nasal acoustic signal processing method in this layer. In addition, it supports the comparison of the left and right sides of the nasal cavity or the nasal cavity before and after treatment,

providing an overall view of the test results. Moreover, it can present the specific cross-sectional area values at key points of the nasal cavity in graphical and tabular form. The software also supports the automatic generation of test reports from the results of these tests. This layer provides a variety of result comparison methods and accurate nasal cavity depth–cross-sectional area values for the data visualization layer.

- In the data visualization layer, the software can generate accurate nasal cavity two-dimensional depth–cross-sectional area curves and render colorful nasal cavity three-dimensional structure reconstruction models. This layer also supports real-time adjustment of the viewing angle and zoom scale of the three-dimensional structure reconstruction models. Based on the multi-dimensional data visualization approach, this layer provides users with intuitive images and detailed data. These images and data, together with test reports, provide abundant analysis results for the information management layer.
- The information management layer is the top layer of the software, which mainly adopts database technology to implement the functions of adding tested persons, editing tested personal information, and deleting tested persons. The analysis results from the data analysis layer and the data visualization layer are integrated and stored with the corresponding tested personal information, which enhances operational efficiency.

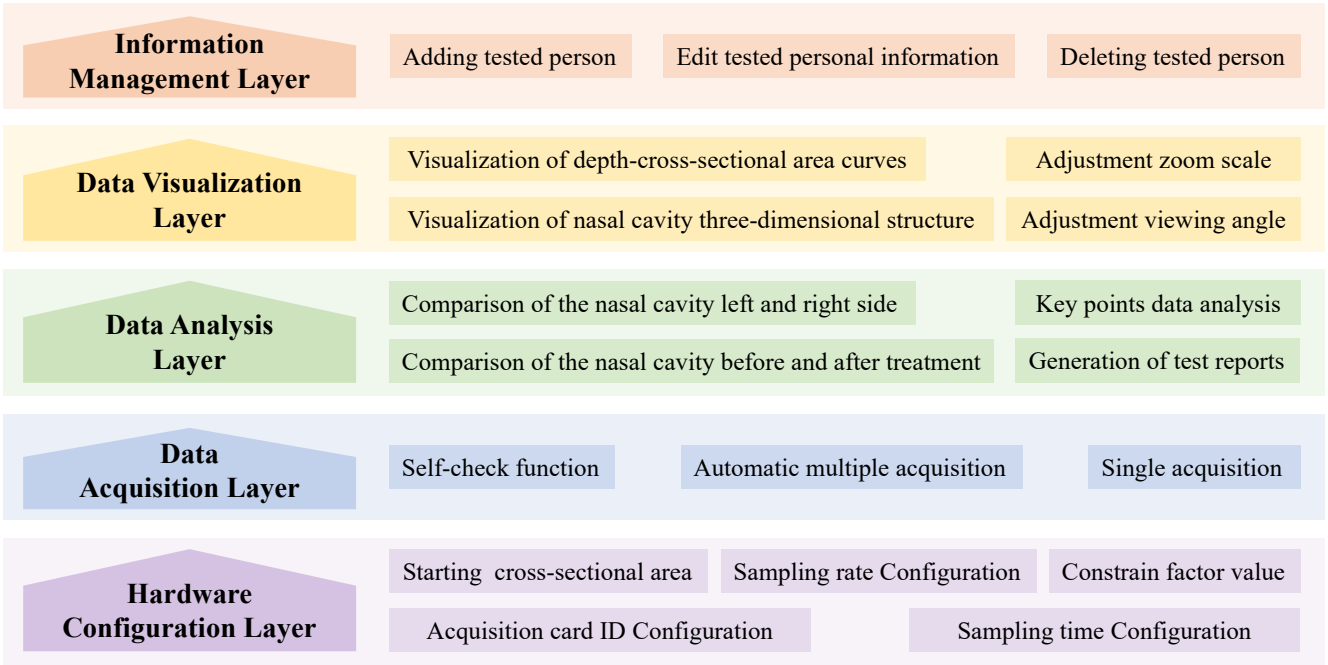


Figure 3. Upper computer software architecture diagram.

3. Nasal Acoustic Signal Processing Methods

The nasal acoustic signal processing method of the upper computer includes the nasal cavity acoustic signal preprocessing method and the nasal cavity three-dimensional structure hierarchical reconstruction method. The nasal cavity acoustic signal preprocessing method involves analyzing the original nasal acoustic signal in both time and frequency domains to generate the input impulse response sequence. This sequence is then utilized as an input for the nasal cavity three-dimensional structure hierarchical reconstruction method, which simplifies the physical structure of the nasal cavity into multiple layers of varying materials. This simplification facilitates the calculation of cross-sectional area values at different depths within the nasal cavity using the input impulse response sequence.

3.1. Nasal Cavity Acoustic Signal Preprocessing Method

The distance between the microphone, the bottom of the tube, and the object to be measured is shorter in a short-source acoustic tube than in a long-source acoustic tube, making it difficult to separate the incident and reflected waves. The nasal cavity acoustic signal preprocessing flow diagram is shown in Figure 4. Firstly, the incident and reflected waves are separated based on the acoustic propagation characteristics of the short-source acoustic tube. The influence of the DC offset component is then eliminated, and high-frequency noise is reduced by introducing a constraint factor, ultimately resulting in a more accurate input impulse response sequence.

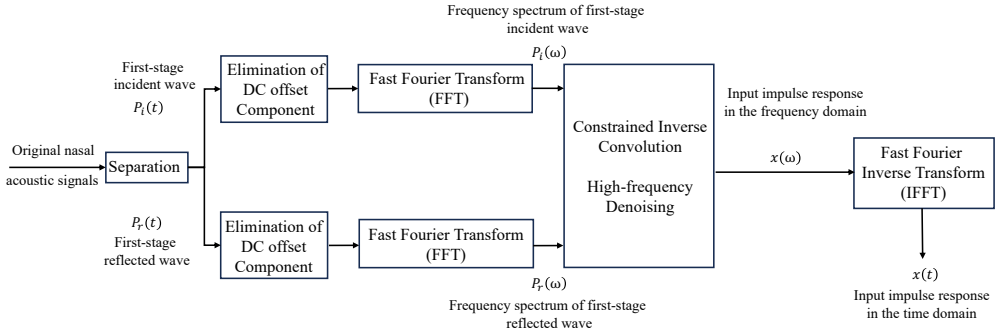


Figure 4. Nasal cavity acoustic signal preprocessing flow diagram.

3.1.1. Separation of Incident and Reflected Waves

The propagation of acoustic waves in a short-source acoustic tube is shown in Figure 5. Initially, the pulsed acoustic waves are generated by the pulse generator at the bottom of the short-source acoustic tube. It propagates upwards through the tube and continues towards the test object after being captured by the microphone for the first time. Upon the pulsed acoustic waves' contact with the surface of the test object, an acoustic wave reflection phenomenon occurs, and some reflected waves return to the short-source acoustic tube, being captured for a second time by the microphone. Subsequently, these waves propagate back down the short-source acoustic tube, undergo reflection at the bottom, and serve as secondary pulsed acoustic waves for the second round of detection of the test object. Due to energy consumption during this cyclic process, the intensity of captured pulsed acoustic waves gradually weakens to zero after multiple rounds of repeated detection.

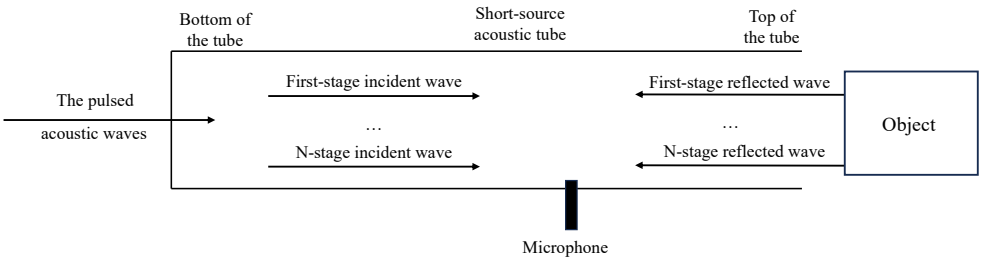


Figure 5. Acoustic wave propagation in a short-source acoustic tube.

Based on the above analysis, it can be concluded that, except for the first captured pulsed acoustic wave, the intensity of each of the two adjacent captured pulsed acoustic waves should be proportional. The $(2n-1)$st captured pulsed acoustic wave is called the n-stage incident wave $(n = 1, 2, ...)$, and the $2n$th captured pulsed acoustic wave is called the n-stage reflected wave $(n = 1, 2, ...)$. Since the first-stage incident wave serves as the original pulsed acoustic wave generated by the pulse generator, the amplitude of the first-stage reflected wave represents the maximum energy, which is beneficial to the enhancement of detection accuracy. Therefore, the separated first-stage incident wave and first-stage reflected wave are used as the incident wave $P_i(t)$ and reflected wave $P_r(t)$ to detect the three-dimensional structure of the nasal cavity.

After separating the incident and reflected waves, the input impulse response $x(t)$ is calculated using the incident wave $P_i(t)$ and the reflected wave $P_r(t)$, and the relationship between the three in the time domain is [16]

$$P_r(t) = \int_0^t x(t-\tau)P_i(\tau)d\tau \quad (1)$$

where τ is the duration of the incident wave. The time domain convolution of the input impulse response and the incident wave is the reflected wave; then, in the frequency domain, the input impulse response is the ratio of the reflected wave to the incident wave:

$$x(\omega) = \frac{P_r(\omega)}{P_i(\omega)} \quad (2)$$

where ω is the discrete angular frequency, $P_i(\omega)$ is the incident wave in the frequency domain, and $P_r(\omega)$ is the reflected wave in the frequency domain. $x(\omega)$ is the input impulse response in the frequency domain, and the input impulse response sequence $x(t)$ in the time domain is calculated by the inverse fast Fourier transform.

When using the reflected and incident waves in the frequency domain to calculate the input impulse response, the division operation in the calculation amplifies the influence of the DC offset component and high-frequency noise, which leads to a large error in the final results of the nasal cavity three-dimensional structure reconstruction and fails to meet the accuracy of practical applications.

3.1.2. Elimination of DC Offset Component From Incident and Reflected Waves

As the electronic components in the nasal acoustic signal acquisition device are susceptible to environmental interference, the DC component from the incident and reflected waves will be shifted. This DC offset component can affect the amplitude range of both the incident and reflected waves, as well as the input impulse response sequence. Consequently, the related parameters in the nasal cavity three-dimensional structure hierarchical reconstruction method are further affected. In the final nasal cavity three-dimensional structure reconstruction, the presence of the DC offset component tends to cause cross-sectional area values at the same depth to exceed standard values. Based on the principles of the acoustic wave reflection method, this phenomenon becomes more pronounced over time. Hence, the elimination of the interference caused by the DC offset component is particularly crucial [17,18].

In this research, before the first-stage incident wave is recorded by the microphone, there exists a segment of acoustic waves, the amplitude of which remains relatively stable. Hence, these values are chosen as the DC offset component. This DC offset component is then separately eliminated in the time domain for both the incident and reflected waves, correcting the amplitude range of the input impulse response to be obtained subsequently. Ultimately, this correction enhanced the accuracy of the nasal cavity three-dimensional structure reconstruction results.

3.1.3. Removal of High-Frequency Noise From Incident and Reflected Waves

When the input impulse response is obtained in the frequency domain, the response includes high-frequency noise. This noise impacts the smoothness of the input impulse response and consequently affects the nasal cavity depth–cross-sectional area curve. This ultimately leads to increased variance between the cross-sectional area values and the standard values, as well as excessive errors at some points, which does not satisfy the accuracy requirement of the nasal cavity three-dimensional structure reconstruction.

As shown in Equation (2), if the acoustic signal is particularly weak near a certain frequency ω_1, i.e., the value of $P_i(\omega_1)$ is very small, then the value of $x(\omega_1)$ will be large. The result of the inverse convolution will greatly amplify the noise at this frequency. Analyzing

the frequency spectrum of the incident wave, it can be seen that the effective frequency spectrum of the incident wave is primarily concentrated within the low-frequency range, with minimal amplitude in the high-frequency spectrum. However, high-frequency signals will be enlarged into high-frequency noise under the effect of the inverse convolution. So, in practice, in order to eliminate the interference of high-frequency noise, Equation (2) is optimized as a constrained inverse convolution [19–21]:

$$x(\omega) = \frac{P_r(\omega)P_i^*(\omega)}{P_i(\omega)P_i^*(\omega) + q} \tag{3}$$

where $P_i^*(\omega)$ denotes the complex conjugate of the incident wave $P_i(\omega)$. The frequency domain separation between the reflected wave $P_r(\omega)$ and the input impulse response $x(\omega)$ is considered an uncertain issue [22,23]. A constraint factor q is introduced in the inverse convolution to prevent the input impulse response from decreasing to the background noise level at high frequencies. Therefore, the role of the constraint factor q is similar to that of a low-pass filter, and the different values of the constraint factor q also have varying degrees of impact on the results of high-frequency noise reduction. In this research, the appropriate value of the constraint factor was found by taking the average of several trials.

3.2. The Nasal Cavity Three-Dimensional Structure Hierarchical Reconstruction Method

In order to identify the relationship between the input impulse response and the cross-sectional areas at various depths within the nasal cavity, a simplified model of the nasal cavity's structure is established by the nasal cavity three-dimensional structure hierarchical reconstruction method. The process of the nasal cavity three-dimensional structure hierarchical reconstruction method is illustrated in Figure 6.

In order to facilitate the calculation, the physical structure of the nasal cavity needs to be simplified. The schematic diagram of acoustic wave propagation in a simplified nasal cavity is shown in Figure 7 [24].

The physical structure of the nasal cavity is simplified to a physical model with more than n elastic planes, where planes 0-n represent the depth of the nasal cavity from shallow to deep. It is assumed that when the pulsed acoustic waves propagate to a space beyond n-th layers, the intensity of the pulsed acoustic waves has already diminished to zero.

To simplify the calculation, the distance between each plane is set to x, measured in centimeters. Each space between two adjacent planes is referred to as a layer. For instance, the area between plane 0 and plane 1 is denoted as layer 1. The signal in each layer can be expressed as a polynomial in the z-transform, $D_i(z)$ is the downward propagating signal in layer i, and $U_i(z)$ is the upward propagating signal in layer i. Specifically, $D_1(z)$ represents the z-transform of the first-stage incident wave, defined as $D_1(z) = 1$, and $U_1(z)$ is the z-transform of the first-stage reflected wave.

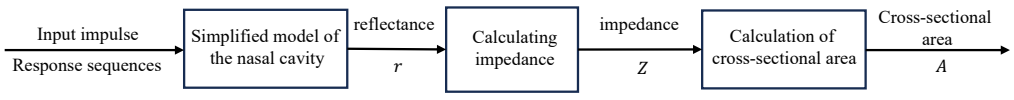


Figure 6. The flow diagram of the nasal cavity three-dimensional structure hierarchical reconstruction.

Pulsed acoustic waves will be reflected and transmitted on each plane, taking the plane i as an example, the transmission–reflection pattern on plane i is shown in Figure 8.

Taking downward propagation as the positive direction, if the incident wave intensity is 1, the reflectance and transmittance on the plane i are r_i and t_i, respectively. As shown on the left side of Figure 8, the reflectance of the incident wave is r_i and the transmittance is t_i. As shown on the right side of Figure 8, the reflectance of the reflected wave is $-r_i$ and the transmittance is $-t_i$. The transmittance and reflectance satisfy Equation (4) [24,25]:

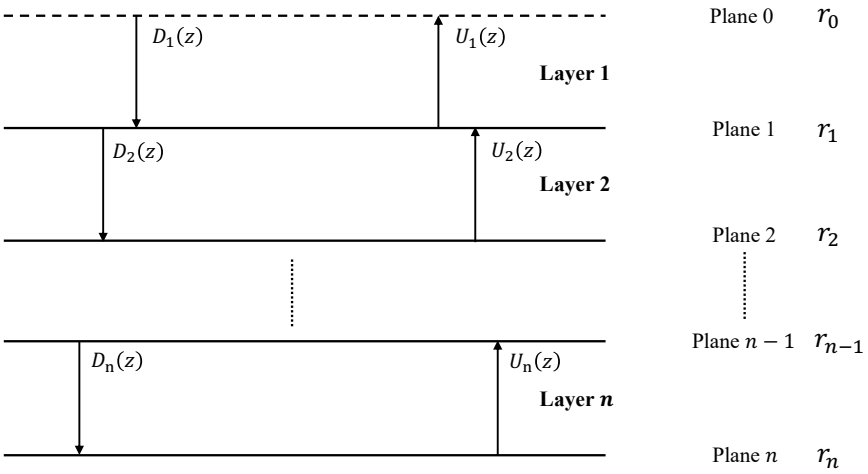


Figure 7. The schematic diagram of the acoustic wave propagation in a simplified nasal cavity.

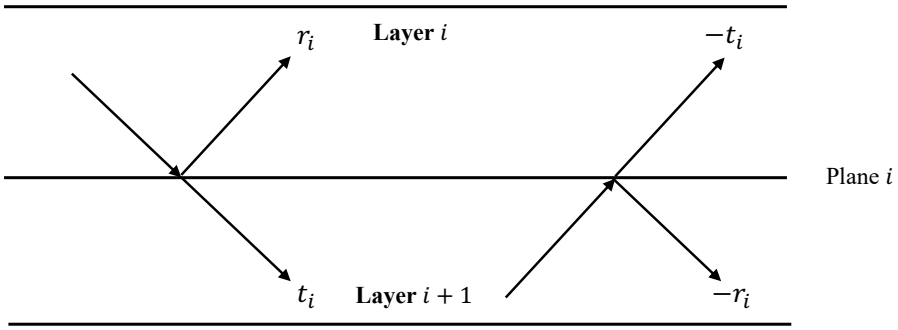


Figure 8. The transmission–reflection pattern on plane i.

$$1 = r_i^2 + t_i^2 \tag{4}$$

Based on the simplified physical properties of the nasal cavity in Figures 7 and 8, the relationship between $D_1(z)$, $U_1(z)$, and $D_{n+1}(z)$, $U_{n+1}(z)$ can be represented as follows [24–26]:

$$\begin{bmatrix} D_{n+1}(z) \\ U_{n+1}(z) \end{bmatrix} = \frac{z^{0.5n}}{\sigma_n} \begin{bmatrix} P_n^R(z) & Q_n^R(z) \\ Q_n(z) & P_n(z) \end{bmatrix} \begin{bmatrix} D_1(z) \\ U_1(z) \end{bmatrix} \tag{5}$$

$$\begin{bmatrix} P_n^R(z) & Q_n^R(z) \\ Q_n(z) & P_n(z) \end{bmatrix} = \prod_{i=1}^{n} \begin{bmatrix} z^{-1} & -r_i \\ -r_i z^{-1} & 1 \end{bmatrix} \tag{6}$$

where $\sigma_n = \prod_{i=1}^{n} t_i$, t_i is the transmittance on plane i, $D_1(z) = 1$, $U_1(z)$ is the z-transform of the first-stage reflected wave, $D_{n+1}(z)$ and $U_{n+1}(z)$ are functions of z and r. Since $D_1(z) = 1$, $U_1(z)$ can be denoted by $U_1(z) = 1 + x_1 z^{-1} + x_2 z^{-2} + ... + x_n z^{-n}$ [25]. Therefore, according to Equations (4)–(6), the reflectance relationship between the input impulse response sequence and different planes can be calculated [25]:

$$r_k = \begin{cases} 0, & k = 0 \\ x_1, & k = 1 \\ \sum_{j=1}^{k-1} P_j(z) x_{k+1-j} \left[\prod_{j=1}^{k-1} (1 - r_j^2) \right]^{-1}, & k = 2, 3, ...n \end{cases} \tag{7}$$

where x_k is the input impulse response intensity value of z^{-k} when the pulsed acoustic wave is reflected plane by plane from plane k back to plane 0. The equation for the relationship between the reflectance and the impedance at different layers of the simplified nasal cavity is:

$$Z_k = Z_0 \prod_{i=0}^{k-1} \frac{1 - r_i}{1 + r_i} \quad k = (1, 2, ..., n + 1) \tag{8}$$

where Z_k is the value of impedance at the k-th layer of the simplified nasal cavity. Z_0 is defined as the atmospheric impedance, the value of which is known. The equation for the relationship between the impedance at different layers of the simplified nasal cavity and the cross-sectional area A is:

$$A(k) = \frac{Z_0}{Z_k} \tag{9}$$

where $A(k)$ is the value of the cross-sectional area at the k-th layer of the simplified nasal cavity, expressed in cm^2.

Ultimately, the cross-sectional area values at different depths of the nasal cavity are calculated from the input impulse response sequence by using the reflectance as an intermediate variable [27].

4. Results and Discussion of the Nasal Cavity Three-Dimensional Structure Reconstruction System

4.1. Results and Analysis of Nasal Acoustic Signal Acquisition

In this experiment, the straight tube model and the simulated nasal cavity model from GM Company in the UK were used as the test objects, respectively. The straight tube model is a metal tube with a constant cross-sectional area and made of 304 stainless steel. This tube is used to assess the average detection precision of the nasal cavity three-dimensional structure reconstruction system. The simulated nasal cavity model is a plastic tube with cross-sectional areas similar to those of a typical human nasal cavity and made of polyvinyl chloride. This tube is used to assess the precision of the system in detecting key points, including the starting point, half-way point, endpoint, minimum area point, and maximum area point. During the actual patient examination, a short glass tube of 5 cm length is inserted into the top of the short-source acoustic tube. This allows the patient's nostril to fit snugly against the glass tube, preventing acoustic waves from propagating into the air where they cannot be adequately captured by the microphone. Thus, in order to simulate the actual examination effect, the first 5 cm of both models are not considered as effective measurement depths. As shown in Figure 9a, the straight tube model has a length of 17 cm, an effective measurement depth of 12 cm, and a cross-sectional area of 1.23 cm^2. As shown in Figure 9b, the simulated nasal cavity model is similar to a cone, the length of the simulated nasal cavity model is 22 cm, and the effective measurement depth is 13 cm. A 4 cm thickness of sponge is inserted from 13 cm to the top of the model to absorb the excess pulsed acoustic waves. The cross-sectional area reaches its maximum value of 8 cm^2 at a valid measurement length of 10.4 cm and a minimum value of 0.5 cm^2 at a valid measurement length of 1.8 cm.

The original nasal acoustic signal in the straight tube model and the simulated nasal cavity model are shown in Figure 10. The horizontal coordinate is the time, and the vertical coordinate is the voltage, which is proportional to the intensity of the acoustic wave. Since the first-stage incident wave has the lowest loss in the short-source acoustic tube and is the earliest pulsed acoustic wave recorded by the microphone. The intensity of the first-stage incident wave should be the maximum. As shown in Figure 10, the maximum peak of the first-stage incident wave is about 0.5 V, both in the straight tube model and the simulated nasal cavity model, and the pulsed acoustic wave oscillates to 0 V gradually with time. As shown in Figure 10, according to the acoustic wave propagation characteristics in a short-source acoustic tube mentioned in Section 3.1.1, it can be seen that the first-stage incident wave is recorded at about 0.8 ms and lasts for 0.8 ms, and the first-stage reflected wave is recorded at about 1.6 ms and lasts for about 1.7 ms.

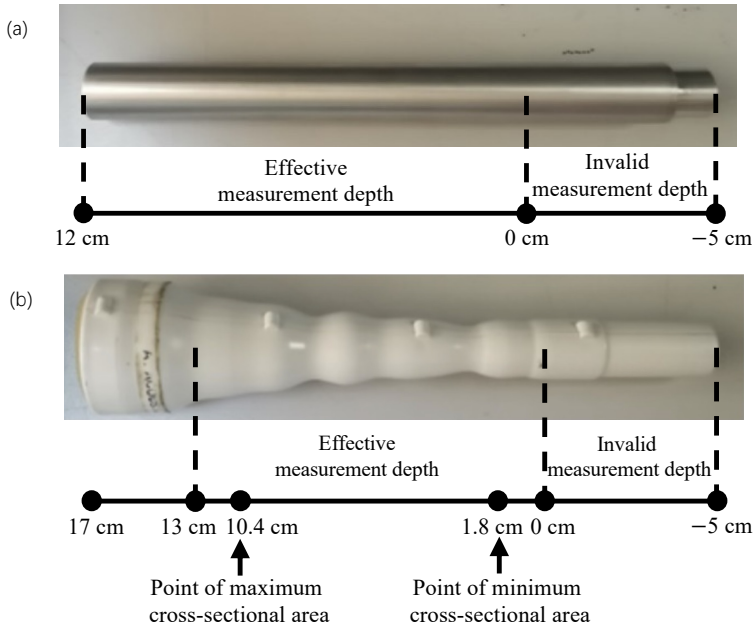


Figure 9. (**a**) The straight tube model. (**b**) The simulated nasal cavity model.

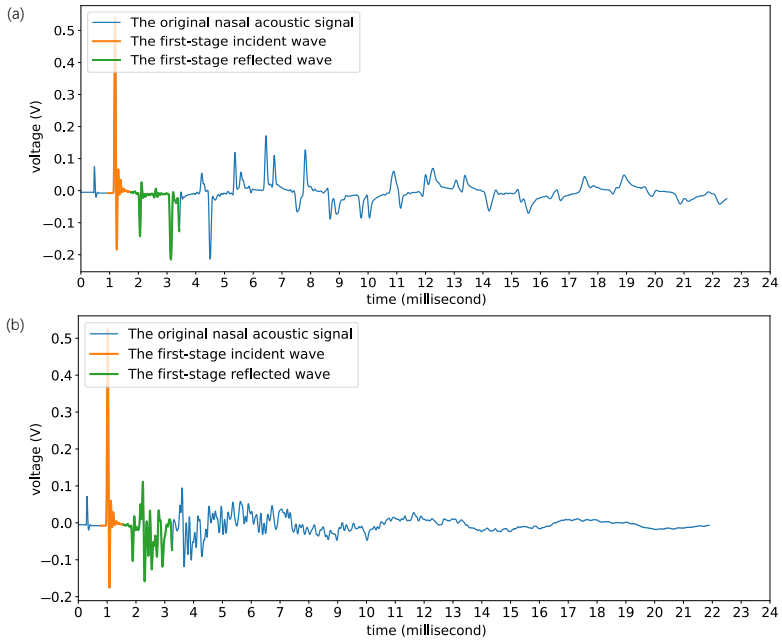


Figure 10. (**a**) Original nasal acoustic signal of the straight tube model. (**b**) Original nasal acoustic signal of the simulated nasal model.

4.2. Results and Analysis of Nasal Acoustic Signal Preprocessing

The first-stage incident wave and the first-stage reflected wave are separated from the original nasal acoustic signal to reconstruct the three-dimensional structure of the nasal cavity. The stable-state voltage value before the peak of the first-stage incident wave is selected as the DC offset component, corrected in the time domain. Subsequently, a Fourier transform is applied to the incident and reflected waves using 255 sample points at a sampling frequency of 100 kHz. The time–domain and frequency–domain plots of the input impulse responses from the straight tube model and the simulated nasal cavity model, both before and after the elimination of the DC offset component, are shown in Figure 11.

From Figure 11, it can be seen that the influence of the DC offset component on the input impulse response primarily appears as changes in amplitude. The reason for this phenomenon is that the DC offset component changes the amplitude of the incident and reflected waves at zero frequency in the frequency domain. This change subsequently modifies the baseline value of the DC component within the input impulse response.

High-frequency noise also affects the input impulse response, which can be eliminated by introducing a constraint factor. Based on the step of eliminating the DC offset component, the time–domain and frequency–domain plots of the input impulse responses from the straight tube model and the simulated nasal cavity model, both before and after the introduction of the constraint factor, are shown in Figure 12.

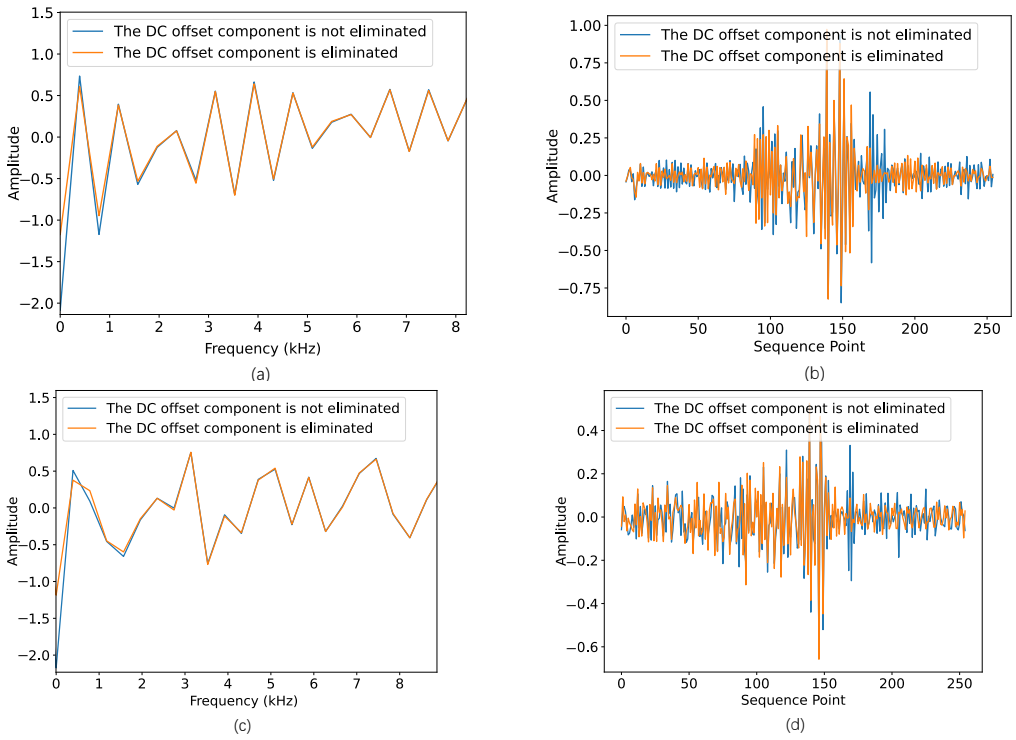


Figure 11. (**a**) Partial input impulse response frequency spectrum of the straight tube model. (**b**) Input impulse response time sequence of the straight tube model. (**c**) Partial input impulse response frequency spectrum of the simulated nasal cavity model. (**d**) Input impulse response time sequences of the simulated nasal cavity model.

From Figure 12, it can be clearly seen that the constraint factor significantly weakens the amplified high-frequency noise during the computational process. Its effect is similar to that of the low-pass filter. The magnitude of the constraint factor determines the frequency band of the noise elimination. When the value of the constraint factor is too small, the high-frequency noise is not eliminated cleanly, resulting in an unsatisfactory denoising effect. This subsequently impacts the amplitude of the input impulse response in later calculations. This eventually leads to an inaccurate result for the final nasal cavity three-dimensional structural reconstruction. Conversely, if the constraint factor is excessively large, it weakens the amplitude of certain low- and medium-frequency bands, resulting in a smoother input impulse response curve. However, some of the low- and medium-frequency characteristics of the input impulse response will be lost. Based on the analysis of the results of several experiments, $q = 0.1$ is chosen for high-frequency denoising. In this setting, it effectively eliminates high-frequency noise from the input impulse response sequence while preserving the overall low- and medium-frequency features.

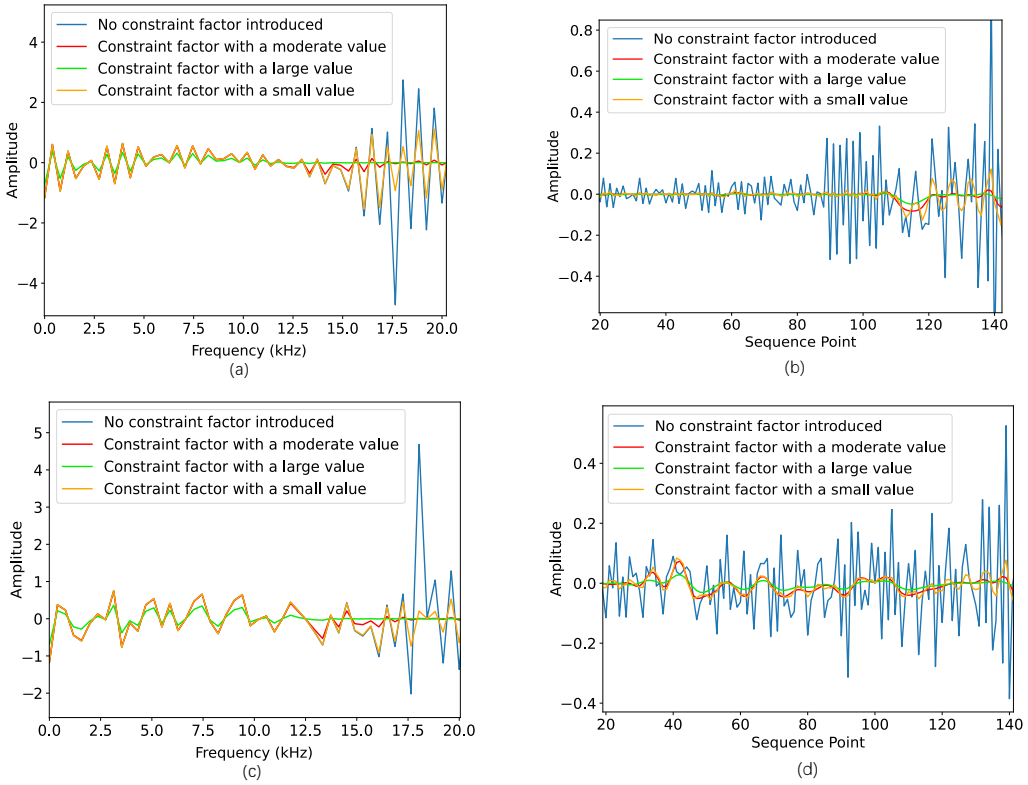


Figure 12. (**a**) Partial input impulse response frequency spectrum of the straight tube model. (**b**) Partial input impulse response time sequence of the straight tube model. (**c**) Partial input impulse response frequency spectrum of the simulated nasal cavity model. (**d**) Partial input impulse response time sequence of the simulated nasal cavity model.

4.3. Results and Analysis of the Nasal Cavity Three-Dimensional Structure Hierarchical Reconstruction Method

The cross-sectional area values of different depths of the nasal cavity were obtained by analyzing the input impulse response sequences using a hierarchical reconstruction method. The standard curves of the two-dimensional depth–cross-sectional area curves were plotted using the actual physical size of the two tested models and compared with the reconstruction results of the original nasal acoustic signals using different preprocessing methods. The reconstruction results for the straight tube model and the simulated nasal cavity model are shown in Figures 13 and 14, respectively.

From Figures 13 and 14, it can be seen that the existence of the DC offset component causes the error in the cross-sectional area to increase as the depth of the nasal cavity increases. The reason for this is that the nasal cavity three-dimensional structure hierarchical reconstruction method is an iterative method that needs to be solved by using the parameters related to the previous depth layer to solve for the current depth layer. If there is an obvious error in the initial value or at a specific point, the error in the final iteration will progressively increase. Moreover, when the value of the constraint factor q is too small, high-frequency noise is also involved in the iterative operation, resulting in poor smoothness of the two-dimensional depth–cross-sectional area curve in the reconstruction. Conversely, when the value of the constraint factor q is too large, the input impulse response sequence curve is under-fitted, which leads to the two-dimensional depth–cross-sectional area curve being too smooth and the amplitude significantly deviating from that of the standard curves. For instance, the simulated nasal cavity model exhibits sharp bends at both the minimum and maximum cross-sectional area points. These sharp bends result in rapid transitions in the cross-sectional area, making it more susceptible to high-frequency noise and the DC offset component. When the constraint factor q is excessively large, it suppresses too

much high-frequency information, resulting in a two-dimensional depth–cross-sectional area curve that is too flat at the bends, failing to reflect the changes at the sharp bends.

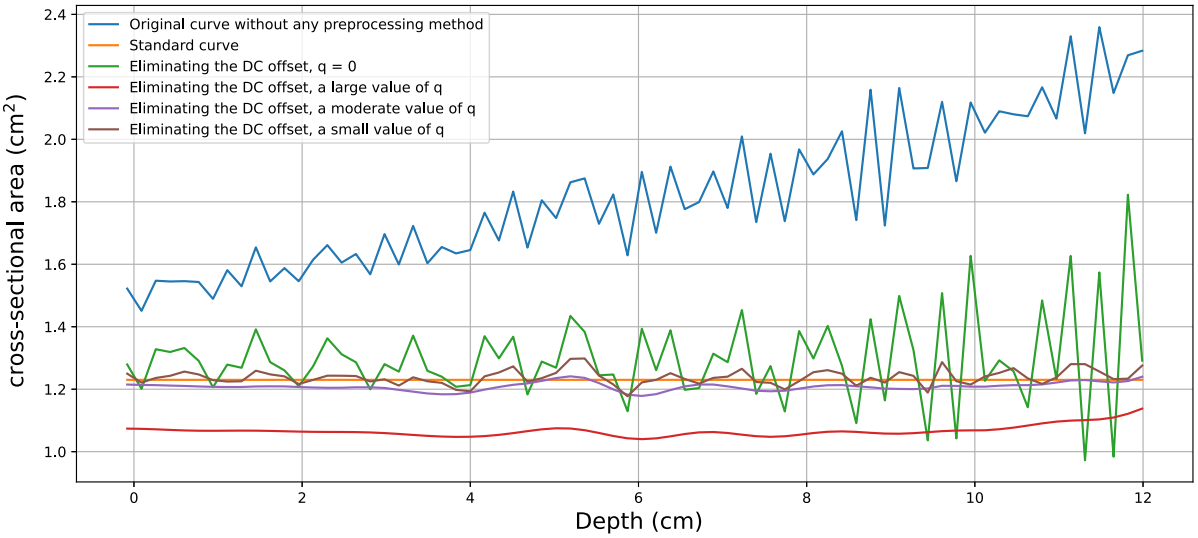


Figure 13. Reconstruction results of two-dimensional depth–cross-sectional area curves of the straight tube model.

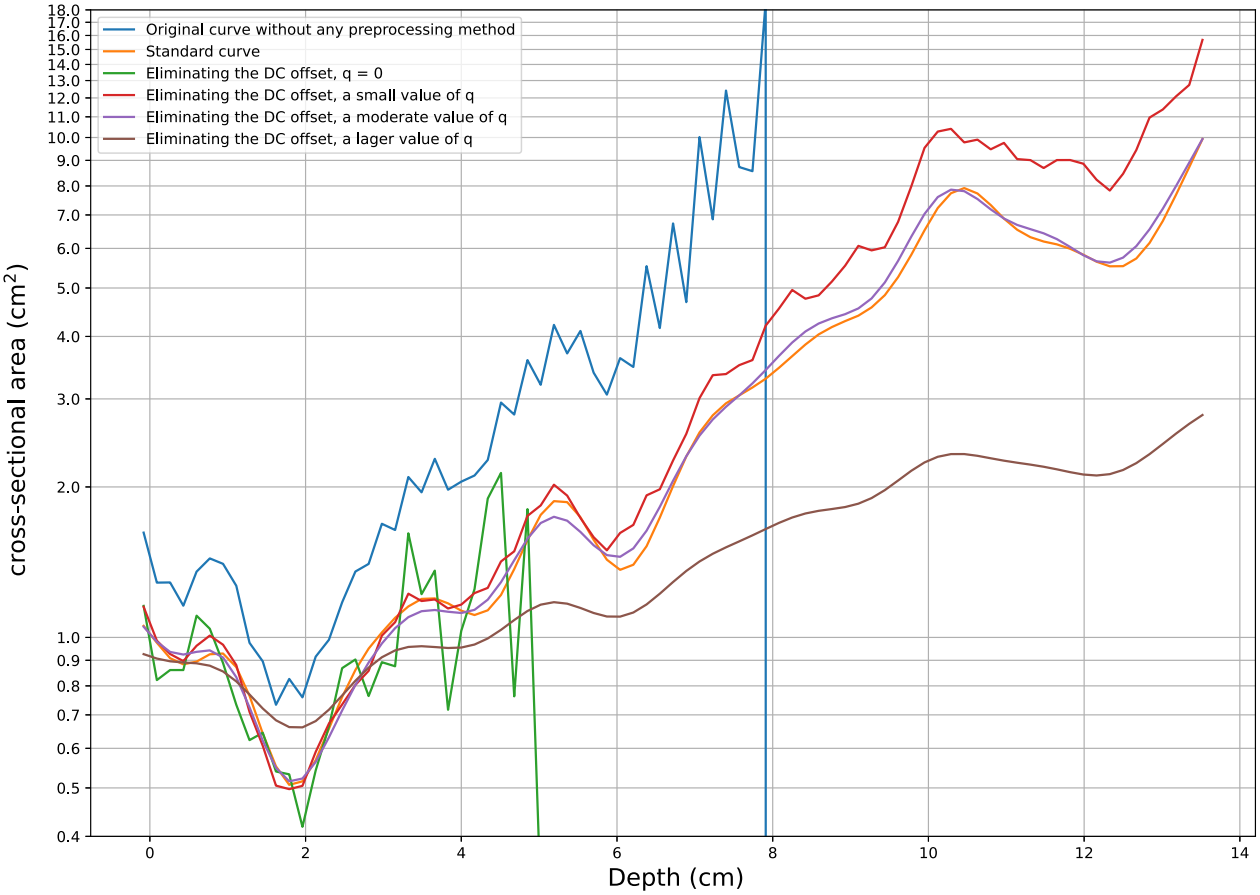


Figure 14. Reconstruction results of two-dimensional depth–cross-sectional area curves of the simulated nasal cavity model.

The error statistics of the reconstructed result and the actual physical model under different preprocessing methods are shown in Tables 1 and 2.

Table 1. Errors in reconstructed results with the straight tube model under different preprocessing methods.

Errors	Preprocessing Methods		
	Uncorrected DC Offset No Constraint Factors Introduced	**Elimination of DC Offset No Constraint Factors Introduced**	**Elimination of DC Offset Moderate Value of Constraint Factor**
Root mean squared error (cm^2)	0.6284	0.1545	0.0201
Maximum relative error (%)	91.8108	48.1741	4.1950
Minimum relative error (%)	17.9650	0.2356	0.0441
Mean relative error (%)	47.6467	9.0237	1.8248

Table 2. Errors in reconstructed results with the simulated nasal cavity model under different preprocessing methods.

Errors	Preprocessing Methods		
	Uncorrected DC Offset No Constraint Factors Introduced	**Elimination of DC Offset No Constraint Factors Introduced**	**Elimination of DC Offset Moderate Value of Constraint Factor**
Root mean squared error (cm^2)	4.7730	3.5619	0.1510
Maximum relative error (%)	681.9042	121.7401	8.7100
Minimum relative error (%)	27.6178	0.3094	0.0163
Mean relative error (%)	107.8128	69.2997	3.3096

From Table 1, it can be seen that the depth–cross-sectional area root mean squared error and mean relative error of the reconstructed result are significantly reduced by eliminating the DC offset component and introducing a moderate value of constraint factor when compared with the actual physical size of the straight tube model. The root mean squared error decreases to 0.0201 cm^2, while the mean relative error reduces to 1.8248%. Compared to the results without any preprocessing method, there is a 96.8014% reduction in root mean squared error and a 45.8219% decrease in mean relative error. Furthermore, the maximum relative error and minimum relative error are significantly reduced. The results show that the depth–cross-sectional error distribution of the reconstructed result is very uniform, and the algorithm has strong stability in the effective measurement depth. From Table 2, it can be seen that all the depth–cross-sectional area error indicators of the reconstructed result are significantly reduced by eliminating the DC offset component and introducing a moderate value of constraint factor when compared with the actual physical size of the simulated nasal cavity model. The root mean squared error decreases to 0.1510 cm^2, while the mean relative error reduces to 3.3096%. Compared to the results without any preprocessing method, there is a 96.8364% reduction in root mean squared error and a 104.5086% decrease in mean relative error. The results show that both the elimination of the DC offset component and a moderate value of constraint factor q can significantly improve the accuracy of the nasal cavity three-dimensional structure hierarchical reconstruction method. However, the above results still contain errors, possibly due to the presence of low-frequency noise, which is difficult to eliminate.

The results of the reconstruction were analyzed in detail using the simulated nasal cavity model, which is more consistent with the actual nasal cavity structure than the straight tube model. Figure 15 shows the relative error of the hierarchical reconstruction results of the simulated nasal cavity model at key measurement points under different preprocessing methods. By eliminating the DC offset component and introducing a moderate value of constraint factor, the method not only extends the effective measurement depth but also improves the reconstruction accuracy of the depth–cross-sectional area. As shown in Figure 15, when the DC offset component is not eliminated or the constraint factor is not introduced, the method is unable to reconstruct the cross-sectional area at a depth of 13 cm because the

increased high-frequency noise is not suppressed. With the elimination of the DC offset component and the introduction of a moderate value of the constraint factor, the effective measurement depth of the nasal cavity reconstruction method is extended to 13 cm, and the correction effect is obvious at the starting point (0 cm), half-way point (7 cm), and the endpoint (13 cm). Compared to the uncorrected DC offset component and not introducing the constraint factor method, the accuracy of the cross-sectional area reconstruction at the starting point is improved by 43%, the relative error at the half-way point is reduced to 1.7% and the accuracy is improved by 178.3%, and the endpoint still maintains a low relative error of 1.9%. In consideration of the nasal cavity three-dimensional structure hierarchical reconstruction method is an iterative method. In this experiment, errors caused by the DC offset component and high-frequency noise will both gradually accumulate. This eventually leads to a significant error in the reconstruction results. When the value of the introduced constraint factor is moderate, the cumulative error caused by high-frequency noise will be significantly reduced, thus improving the reconstruction accuracy at deeper distances. In addition, the accuracy of the method at the minimum and maximum cross-sectional area points is improved by 44.1% and 224%, respectively.

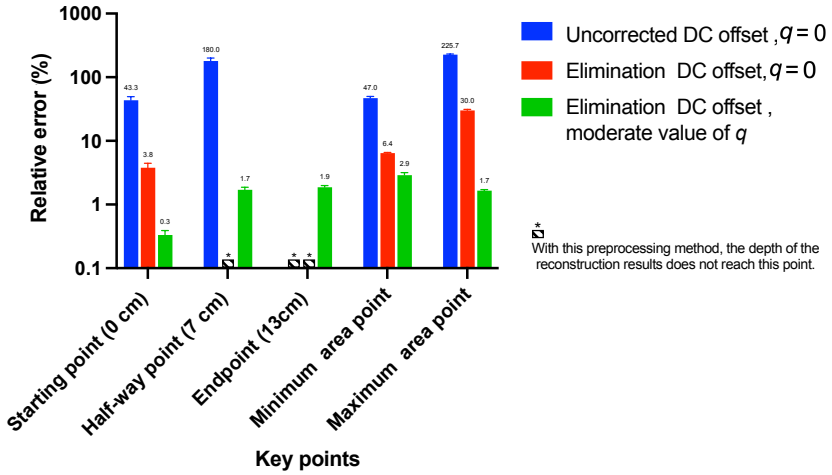


Figure 15. Relative errors of key points in reconstructed results with a simulated nasal cavity model under different preprocessing methods.

Comparison of the acoustic wave reflection method based on the long-source acoustic tube [28] with MRI and CT shows that the cross-sectional areas measured in the first 7 cm of the nasal cavity are in good agreement [27,28]. However, the cross-sectional areas measured by the acoustic wave reflection method based on the long-source acoustic tube after 7 cm were significantly larger than those measured by CT and MRI. The nasal cavity three-dimensional structure reconstruction system based on the short-source acoustic tube of this research has a mean relative error of 3.3096% in the cross-sectional area of the first 13 cm of the simulated nasal cavity model, and the error of the volume from 0 to 10 cm with the simulated nasal cavity model is 2.5%, which greatly extends the measurement depth of the acoustic wave reflection method.

In order to facilitate the observation of the local features of the reconstructed results, the depth–cross-sectional area curves of the straight tube model and the simulated nasal cavity model are visualized in a three-dimensional view with the elimination of the DC offset component and the moderate value of the constraint factor. The results of the three-dimensional structure reconstruction of the two tested models are shown in Figure 16. The three-dimensional structure reconstruction of the nasal cavity is displayed in different colors according to the size of the radius, and the reconstruction results are displayed more intuitively and stereoscopically. This reconstruction can not only provide a basis for further auxiliary diagnoses of the disease but also facilitate doctors in explaining the physiological structures and pathological characteristics to patients.

4.4. Key Functional Interface of Upper Computer Software Platform

The key functional interface diagram of the upper computer software platform is shown in Figure 17. It shows the lower computer parameter configuration interface, data acquisition interface, single test result analysis interface, multiple left and right nasal cavities test result comparison analysis interface, and nasal cavity three-dimensional structure reconstruction interface in the software, respectively. Shown in Figure 17a is the parameter configuration interface of the lower computer. Parameters such as sampling rate and sampling time can be set to control the collection effect of the lower computer. Shown in Figure 17b is the data acquisition interface. In this interface, the left/right nasal cavity and the number of tests can be selected, and the curve of each test is displayed in real time. Shown in Figure 17c is the single test result analysis interface. The depth–cross-sectional area curve is displayed in detail on this interface, reflecting the variation trend of the cross-sectional area of the nasal cavity at different depths. Moreover, the detailed depth and cross-sectional area values of the first and second narrow points are shown in a table. Shown in Figure 17d is the multiple left and right nasal cavities test result comparison analysis interface. In this interface, according to international medical standards, the red line is used to represent the test curve of the right nasal cavity, and the blue line is used to represent the test curve of the left nasal cavity. It can display the results of multiple tests separately and utilize depth as a standard to concatenate the left and right results curves, highlighting the differences in cross-sectional areas at the same depth between the left and right nasal cavities. Shown in Figure 17e is the nasal cavity three-dimensional structure reconstruction interface. In this interface, different colors are used to distinguish varying cross-sectional areas. At the same time, it also supports real-time adjustment of the viewing angle and zoom scale so that the nasal cavity's three-dimensional structure can be shown more vividly.

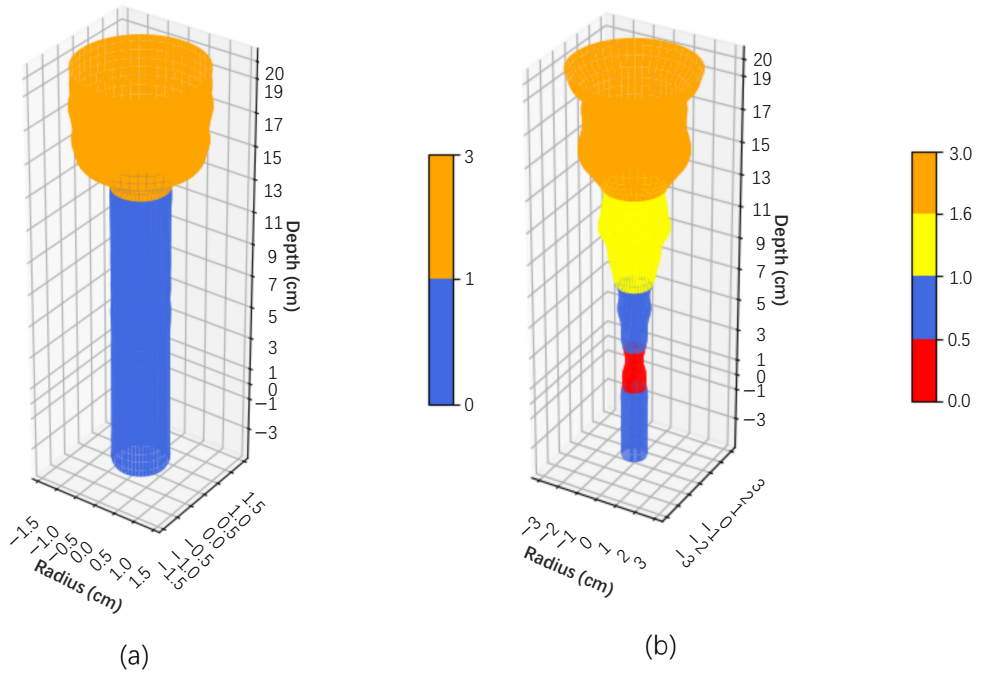
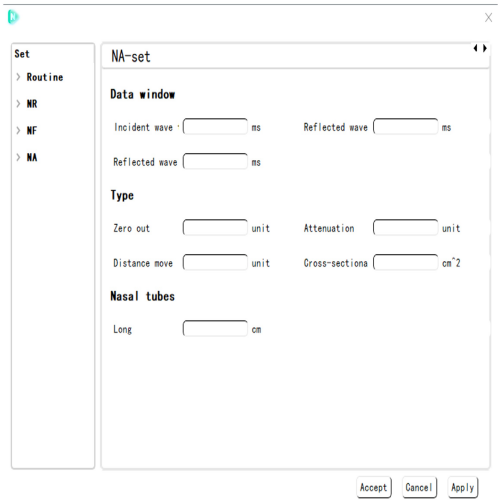
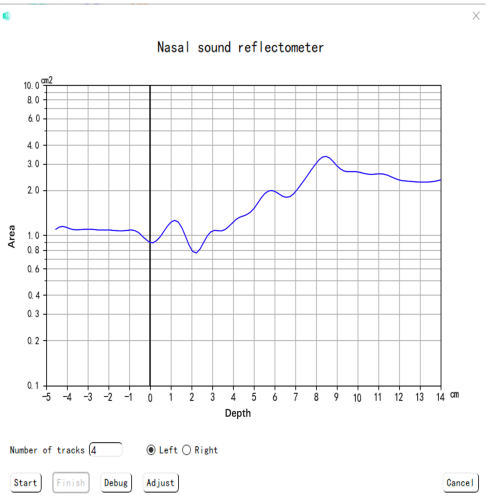


Figure 16. (**a**) The three-dimensional structure reconstruction of the straight tube model. (**b**) The three-dimensional structure reconstruction of the simulated nasal cavity model.

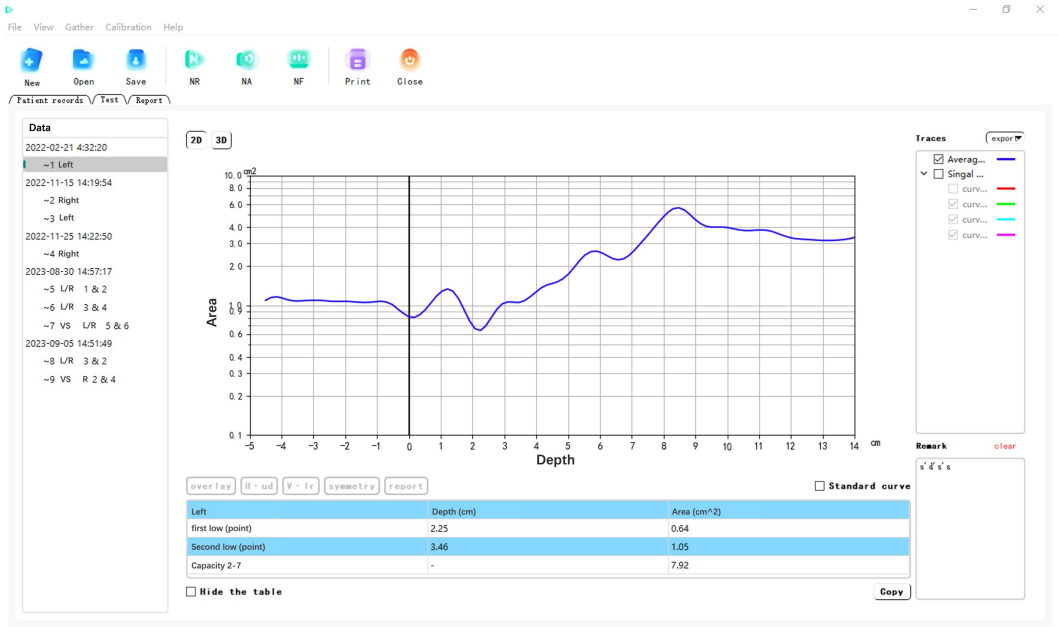
(a)


Set
Routine
NR
NF
NA
NA-set
Data window
Incident wave
ms
Reflected wave
ms
Reflected wave
ms
Type
Zero out
unit
Attenuation
unit
Distance move
unit
Cross-sectiona
cm^2
Nasal tubes
Long
cm
Accept
Cancel
Apply

(b)


Nasal sound reflectometer
Area
Depth
cm
Number of tracks
Left
Right
Start
Finish
Debug
Adjust
Cancel

(c)


File View Gather Calibration Help
New
Open
Save
NR
NA
NF
Print
Close
Patient records
Test
Report
Data
2022-02-21 4:32:20
~1 Left
2022-11-15 14:19:54
~2 Right
~3 Left
2022-11-25 14:22:50
~4 Right
2023-08-30 14:57:17
~5 L/R 1 & 2
~6 L/R 3 & 4
~7 VS L/R 5 & 6
2023-09-05 14:51:49
~8 L/R 3 & 2
~9 VS R 2 & 4
2D
3D
Area
Depth
Traces
Remark
clear
overlay
H - ud
V - lr
symmetry
report
Standard curve
Left
Depth (cm)
Area (cm^2)
first low (point)
2.25
0.64
Second low (point)
3.46
1.05
Capacity 2-7
-
7.92
Hide the table
Copy

(d)


File View Gather Calibration Help
New
Open
Save
NR
NA
NF
Print
Close
Patient records
Test
Report
Data
Test 5
Test 6
Left
Right
Area
Depth
Traces
Remark
clear
overlay
H - ud
V - lr
symmetry
report
Standard curve
Type
position
Capacity 2-7
Capacity 3-5
Capacity 4-8
Area 5
Area 7
Area 3
Area 2
Lowest 1
Depth 1
Lowest 2
Depth 2
Base line
#5 Left
7.92
2.39
9.65
1.75
2.43
1.03
0.66
0.64
2.25
1.05
3.46
#5 Right
6.33
2.22
7.26
1.65
2.08
0.97
0.53
0.49
1.90
1.12
4.15
L + R
14.26
4.61
16.91
3.40
4.51
2.00
1.19
1.14
-
2.18
-
Hide the table
Copy

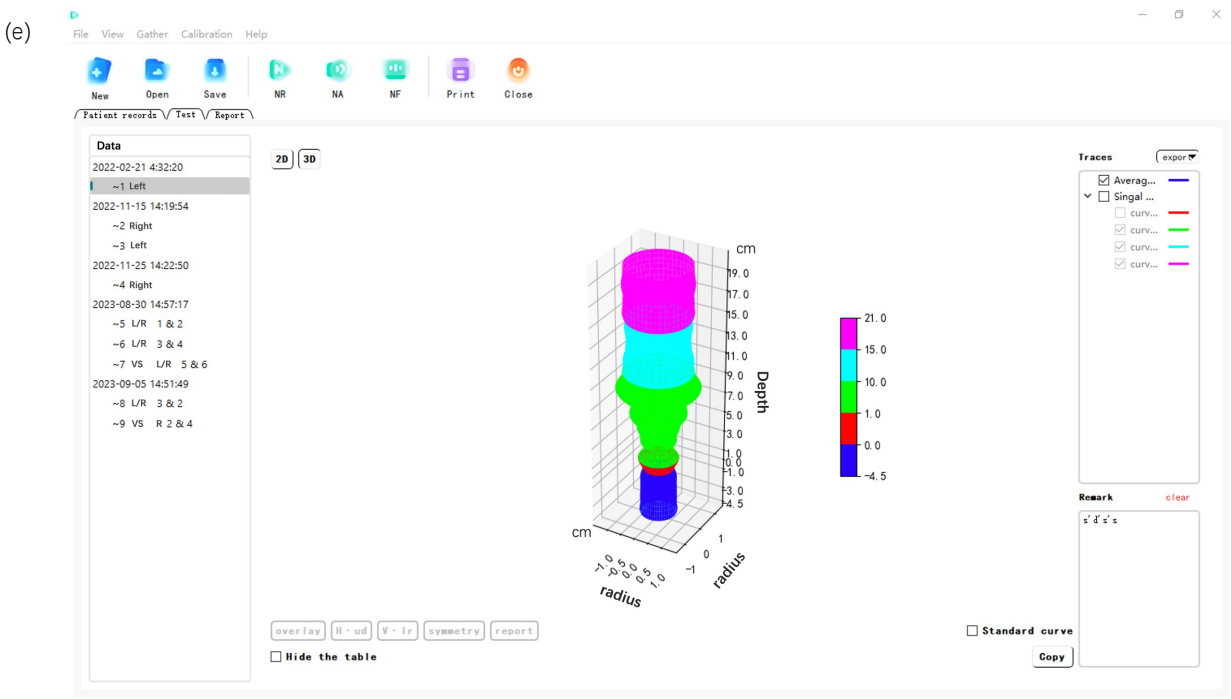


Figure 17. (**a**) Lower computer parameter configuration interface. (**b**) Data acquisition interface. (**c**) Single test result analysis interface. (**d**) Multiple left and right nasal cavities test result comparison analysis interface. (**e**) Nasal cavity three-dimensional structure reconstruction interface.

5. Conclusions

In this research, a system was designed for the nasal cavity three-dimensional structure reconstruction, including the lower computer of a nasal acoustic signal acquisition device and the upper computer of nasal acoustic signal analysis software. The original nasal acoustic signal was obtained by the lower computer of the nasal acoustic signal acquisition device, based on a short-source acoustic tube. The incident and reflected waves were separated from the original nasal acoustic signal according to the propagation characteristics of the acoustic wave in the short-source acoustic tube. The influence of the DC offset component and high-frequency noise on the accuracy of the nasal cavity three-dimensional structure reconstruction was analyzed. After multiple experiments and analysis, the DC offset component was eliminated, and the high-frequency noise was suppressed by introducing the constraint factor q, which is the most important factor for the reconstruction of the nasal cavity. The results show that the accuracy of the nasal cavity three-dimensional structure reconstruction is improved under this system, and the upper computer software is designed to visualize and display the data of the nasal cavity two-dimensional depth–cross-sectional area curves, the nasal cavity three-dimensional structure reconstruction model, and the cross-sectional area values of key points.

The system of this article applies to a nasal cavity three-dimensional structure reconstruction based on a short-source acoustic tube. In actual applications, this system automatically processes and analyzes the collected data, suppressing the impact of high-frequency noise and the DC offset component to better reconstruct the patient's nasal structure. At present, there are still some problems with nasal cavity three-dimensional structure reconstruction based on the acoustic wave reflection method. Building on the foundation laid by this research, the accuracy of the system can be further improved by several methods. First, the impact of low-frequency noise also needs to be considered. However, the removal of low-frequency noise is difficult. In addition, the nasal cavity three-dimensional structure hierarchical reconstruction method relies on past data and has an effect of error accumulation. These are the difficulties that still need to be overcome in nasal cavity three-dimensional structure hierarchical reconstruction methods.

Author Contributions: Conceptualization, X.L., G.M. and C.G.; methodology, X.L., G.M. and C.G.; software, X.L., G.M. and Y.W. (Yuqiao Wang); validation, X.L. and G.M.; formal analysis, C.G.; investigation, G.M. and Y.W. (Yuqiao Wang); resources, X.L. and C.G.; data curation, Y.W. (Yelan Wu), G.M. and W.G.; writing—original draft preparation, X.L., G.M. and C.G.; writing—review and editing, X.L., G.M. and C.G.; visualization, G.M.; supervision, C.G., Y.G. and J.L.; project administration, X.L. and C.G.; funding acquisition, X.L. and C.G. All authors have read and agreed to the published version of the manuscript.

Funding: This research was supported by the Beijing Natural Science Foundation (No. 6214034).

Institutional Review Board Statement: Not applicable.

Informed Consent Statement: Not applicable.

Data Availability Statement: The data that support the findings of this study are available from the corresponding author upon reasonable request. The data are not publicly available due to their containing information that could compromise the privacy of research participants.

Conflicts of Interest: The authors declare no conflicts of interest.

References

1. Castro, P.; Matos, A.; Werner, H.; Lopes, J.; Ribeiro, G.; Araujo, E., Jr. Evaluation of fetal nasal cavity in bilateral congenital dacryocystocele: 3D reconstruction and virtual navigation by magnetic resonance imaging. *Ultrasound Obstet. Gynecol.* **2020**, *55*, 141–143. [CrossRef] [PubMed]
2. Hazeri, M.; Faramarzi, M.; Sadrizadeh, S.; Ahmadi, G.; Abouali, O. Regional deposition of the allergens and micro-aerosols in the healthy human nasal airways. *J. Aerosol Sci.* **2021**, *152*, 105700. [CrossRef] [PubMed]
3. Siu, J.; Dong, J.; Inthavong, K.; Shang, Y.; Douglas, R.G. Quantification of airflow in the sinuses following functional endoscopic sinus surgery. *Rhinology* **2020**, *58*, 257–265. [CrossRef] [PubMed]
4. Zwicker, D.; Yang, K.; Melchionna, S.; Brenner, M.P.; Liu, B.; Lindsay, R.W. Validated reconstructions of geometries of nasal cavities from CT scans. *Biomed. Phys. Eng. Express* **2018**, *4*, 045022. [CrossRef]
5. Mittal, A.K.; Kumar, V.; Kumar, S.; Mahawar, V.; Chowdhury, I.; Agarwal, M. To Assess the Utility of Nasal Magnetic Resonance Imaging in Identifying Clearer Nasal Cavity During Pre-operative Nasal Cavity Assessment. *J. Maxillofac. Oral Surg.* **2022**. [CrossRef]
6. Hao, S.; Wang, N.; Gao, G.; Wang, J.; Bao, W. CT and MRI manifestations of sinonasal neurilemmoma. *Chin. J. Med Imaging Technol.* **2023**, *39*, 342–345.
7. Kim, Y.; Kim, H.J.; Kim, C.H.; Kim, J. CT and MR imaging findings of sinonasal schwannoma: A review of 12 cases. *Am. J. Neuroradiol.* **2013**, *34*, 628–633. [CrossRef]
8. Yang, B.; Wang, Z.; Liu, S.; Xian, J.; Chen, Q.; Liu, Z.; Lan, B. CT and MRI appearance of schwannoma in the sinonasal region. *Chin. J. Radiol.* **2008**, *42*, 618–622.
9. Fujimoto, Y.; Huang, J.; Fukunaga, T.; Kato, R.; Higashino, M.; Shinomiya, S.; Kitadate, S.; Takahara, Y.; Yamaya, A.; Saito, M.; et al. A three-microphone acoustic reflection technique using transmitted acoustic waves in the airway. *J. Appl. Physiol.* **2013**, *115*, 1119–1125. [CrossRef]
10. Wang, J.J.; Chiang, Y.F.; Jiang, R.S. Influence of Age and Gender on Nasal Airway Patency as Measured by Active Anterior Rhinomanometry and Acoustic Rhinometry. *Diagnostics* **2023**, *13*, 1235. [CrossRef]
11. Sharp, D. Increasing the length of tubular objects that can be measured using acoustic pulse reflectometry. *Meas. Sci. Technol.* **1998**, *9*, 1469. [CrossRef]
12. Marshall, I. The production of acoustic impulses in air. *Meas. Sci. Technol.* **1990**, *1*, 413–418. [CrossRef]
13. Li, A. *Improvements to the Acoustic Pulse Reflectometry Technique for Measuring Duct Dimensions*; Open University: Milton, UK, 2004.
14. Marshall, I. Acoustic reflectometry with an arbitrarily short source tube. *J. Acoust. Soc. Am.* **1992**, *91*, 3558–3564. [CrossRef]
15. Buenting, J.E.; Dalston, R.M.; Drake, A.F. Nasal cavity area in term infants determined by acoustic rhinometry. *Laryngoscope* **1994**, *104*, 1439–1445. [CrossRef] [PubMed]
16. Forbes, B.J.; Sharp, D.B.; Kemp, J.A.; Li, A. Singular system methods in acoustic pulse reflectometry. *Acta Acust. United Acust.* **2003**, *89*, 743–753.
17. Vazquez, E.; Pierluissi, J. Acoustic reflectometry for an in vitro model of a human upper airway using sinusoidal wave packets and the Ware–Aki algorithm. *Comput. Methods Biomech. Biomed. Eng.* **2014**, *17*, 119–127. [CrossRef] [PubMed]
18. Ceron, E.R.V. *Acoustic Reflectometry using Gaussian-Modulated Sinusoidal Waves and the Ware-Aki Algorithm*; The University of Texas at El Paso: El Paso, TX, USA, 2010.
19. Sharp, D.B. Acoustic pulse reflectometry: A review of the technique and some future possibilities. In Proceedings of the 8th International Congress on Sound and Vibration, Hong Kong, China, 2–6 July 2001; Citeseer: Princeton, NJ, USA, 2001.
20. Jackson, A.C.; Butler, J.P.; Millet, E.J.; Hoppin, F.G., Jr.; Dawson, S.V. Airway geometry by analysis of acoustic pulse response measurements. *J. Appl. Physiol.* **1977**, *43*, 523–536. [CrossRef]

21. Buick, J.; Kemp, J.; Sharp, D.; Van Walstijn, M.; Campbell, D.; Smith, R. Distinguishing between similar tubular objects using pulse reflectometry: A study of trumpet and cornet leadpipes. *Meas. Sci. Technol.* **2002**, *13*, 750–757. [CrossRef]
22. Man, M. Acoustical Inverse Problem for the Cochlea. *J. Acoust. Soc. Am.* **1981**, *69*, *500–504.*
23. Sondhi, M.M.; Resnick, J. The inverse problem for the vocal tract: Numerical methods, acoustical experiments, and speech synthesis. *J. Acoust. Soc. Am.* **1983**, *73*, 985–1002. [CrossRef]
24. Bardan, V.; Robinson, E.A. Inverse problem for Goupillaud-layered earth model and dynamic deconvolution. *Geophys. Prospect.* **2018**, *66*, 1441–1456. [CrossRef]
25. Ware, J.A.; Aki, K. Continuous and discrete inverse-scattering problems in a stratified elastic medium. I. Plane waves at normal incidence. *J. Acoust. Soc. Am.* **1969**, *45*, 911–921. [CrossRef]
26. Santosa, F.; Schwetlick, H. The inversion of acoustical impedance profile by methods of characteristics. *Wave Motion* **1982**, *4*, 99–110. [CrossRef]
27. Slob, E.; Wapenaar, K.; Treitel, S. Tutorial: Unified 1D inversion of the acoustic reflection response. *Geophys. Prospect.* **2020**, *68*, 1425–1442. [CrossRef]
28. Hilberg, O.; Jackson, A.; Swift, D.; Pedersen, O. Acoustic rhinometry: Evaluation of nasal cavity geometry by acoustic reflection. *J. Appl. Physiol.* **1989**, *66*, 295–303. [CrossRef]

Disclaimer/Publisher's Note: The statements, opinions and data contained in all publications are solely those of the individual author(s) and contributor(s) and not of MDPI and/or the editor(s). MDPI and/or the editor(s) disclaim responsibility for any injury to people or property resulting from any ideas, methods, instructions or products referred to in the content.